NASA Technical Memorandum 104006

USAATCOM Technical Report 92-A-014

An Examination of the Aerodynamic Moment on Rotor Blade Tips Using Flight Test Data and Analysis

Thomas H. Maier and William G. Bousman

October 1993

US ARMY
AVIATION and
TROOP COMMAND

NASA
National Aeronautics and
Space Administration

NASA Technical Memorandum 104006 USAATCOM Technical Report 92-A-014

An Examination of the Aerodynamic Moment on Rotor Blade Tips Using Flight Test Data and Analysis

Thomas H. Maier and William G. Bousman, Aeroflightdynamics Directorate, U. S. Army Aviation and Troop Command, Ames Research Center, Moffett Field, California

October 1993

US ARMY
AVIATION and
TROOP COMMAND

NASA
National Aeronautics and
Space Administration

Ames Research Center
Moffett Field, California 94035-1000

1 SUMMARY

The analysis CAMRAD/JA is used to model two aircraft, a Puma with a swept-tip blade and a UH-60A Black Hawk. The accuracy of the analysis in predicting the torsion loads is assessed by comparing the predicted loads with measurements from flight tests. The influence of assumptions in the analytical model is examined by varying model parameters and comparing the predicted results to baseline values for the torsion loads. Flight test data from a research Puma are used to identify the source of torsion loads. These data indicate that the aerodynamic section moment in the region of the blade tip dominates torsion loading in high-speed flight. Both the aerodynamic section moment at the blade tip and the pitch-link loads are characterized by large positive (nose-up) moments in the first quadrant with rapid reversal of load so that the moment is negative in the second quadrant. Both the character and magnitude of this loading are missed by the CAMRAD/JA analysis.

2 INTRODUCTION

Helicopter power required, fuselage vibration, and rotor structural loads all increase as airspeed is increased to the limit of the flight envelope. In a well-designed aircraft, the maximum airspeed in level, forward flight corresponds to the transmission or engine power limit rather than to a vibration or structural load limit so that helicopter performance is not limited by the aircraft structure. The design of a new rotorcraft requires knowledge of this rotor loading environment to ensure that the rotor or fuselage structure does not limit aircraft performance for normal operating missions. Knowledge of the rotor loading environment is typically based on measurements obtained from previous flight development programs. This method of obtaining design loads for new aircraft does not encourage substantial changes from previous designs. Ideally, comprehensive helicopter analyses should be improved to the point where they can be used to accurately predict design loads from first principles, thus decreasing the risk associated with innovative designs.

The development of comprehensive analyses to the level where the analytical predictions of the rotor loads are trustworthy requires careful testing of

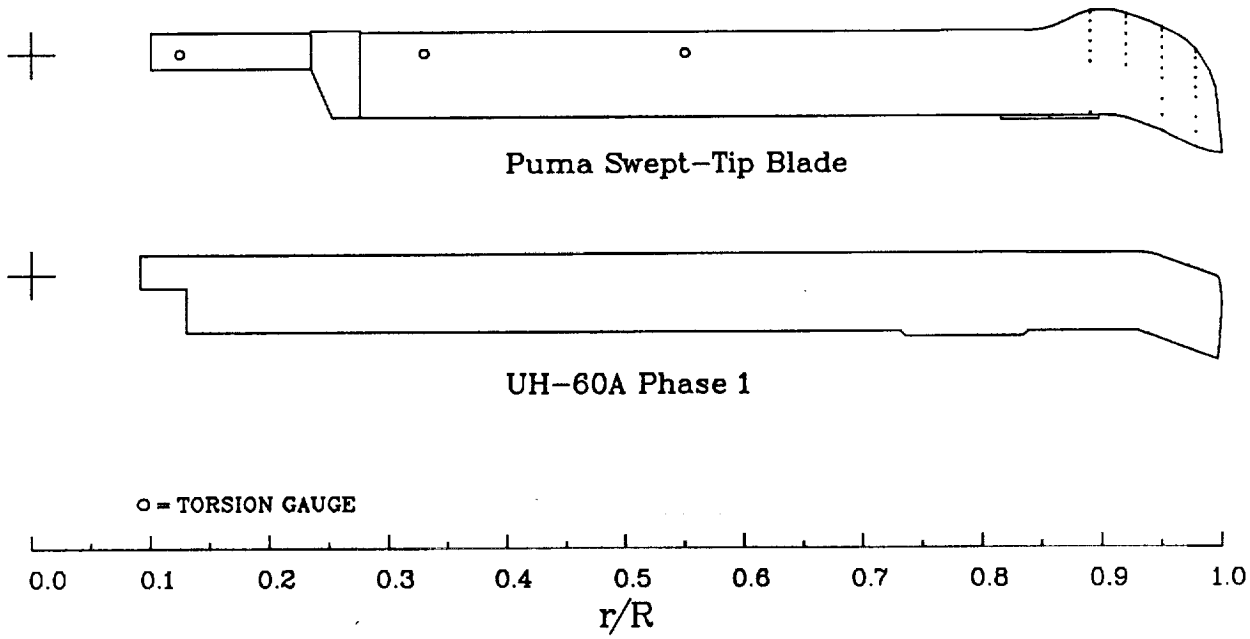

Figure 1. Research Puma and UH-60A blade planforms. Puma pressure arrays shown by dots and torsion moment bridges by open circles.

these methods against appropriate experimental measurements obtained in flight or in the wind tunnel. Reference 1 approached the task of obtaining the appropriate experimental measurements by comparing the rotor loads measured on a variety of different helicopters. Similarities observed in the rotor loading for these different aircraft, then, represent the basic physics of the rotor loads problem and hence provide a good first test for the comprehensive methods. The focus of the present paper is the prediction of blade torsional loading, particularly at high speed. The paper first compares the predictions of the CAMRAD/JA analysis with measurements obtained in flight tests of two helicopters. Then, a number of modeling changes are made in the analysis to better understand the differences that are seen between the predictions and measurements. Available flight test data are then examined in detail to determine what features of the analysis must be improved to obtain satisfactory prediction of the torsion loading.

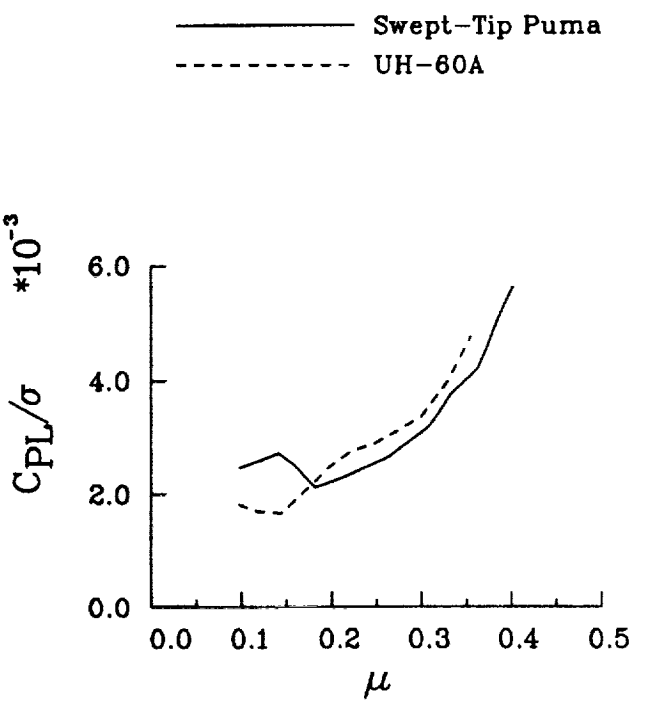

Figure 2. Comparison of oscillatory pitch-link load measurements with advance ratio from the swept-tip Puma and UH-60A; $C_T/\sigma = 0.070$ (Flight 525) for the Puma and $C_T/\sigma = 0.080$ (Flight 9) for the UH-60A; 1–64 harmonics.

3 FLIGHT TEST DATA

The research Puma data used here are part of a large database obtained over a number of years at the Defence Research Agency (DRA) in Bedford, England (formerly the Royal Aerospace Establishment) (ref. 2). The data were obtained under a joint Anglo–French program and have not been published. The blade used on the research Puma is illustrated in figure 1. The rectangular tip of the standard Puma blade has been modified to provide the tip planform shown in the figure. Absolute pressures were measured on the upper and lower surfaces of the modified section at $0.92R$, $0.95R$, and $0.978R$ and upper surface pressures only at $0.89R$. Pitch-link load measurements were made as well as torsion moment measurements at three stations on the blade, as indicated in the figure. A single revolution of data was taken for each flight test point; therefore, there is no averaging of the data. The data were sampled at 256 points over each revolution, which provides a bandwidth of 128 harmonics (azimuthal resolution of 1.4°).

The UH-60A data used here were obtained in a NASA/Army flight test in 1987 (ref. 3) and are stored in an electronic database. The blade tested is illustrated in figure 1 and is identical to the standard UH-60A

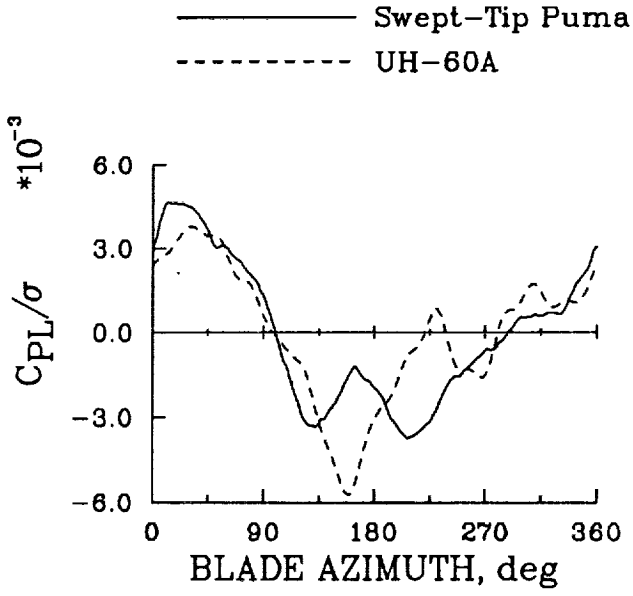

Figure 3. Comparison of pitch-link load measurements with azimuth from the swept-tip Puma and UH-60A; $\mu = 0.362$ and $C_T/\sigma = 0.070$ (Flight 525) for the Puma and $\mu = 0.355$ and $C_T/\sigma = 0.080$ (Flight 9) for the UH-60A; 1–64 harmonics.

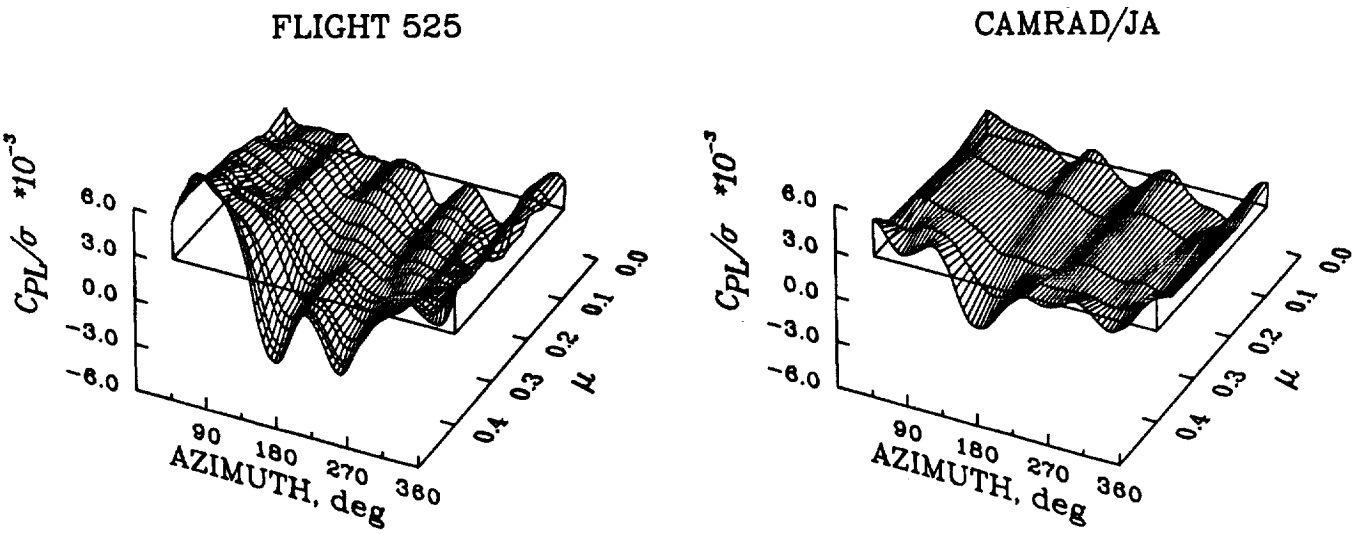

Figure 4. Comparison of oscillatory pitch-link load for the swept-tip Puma as a function of azimuth and advance ratio (Flight 525); 1–12 harmonics.

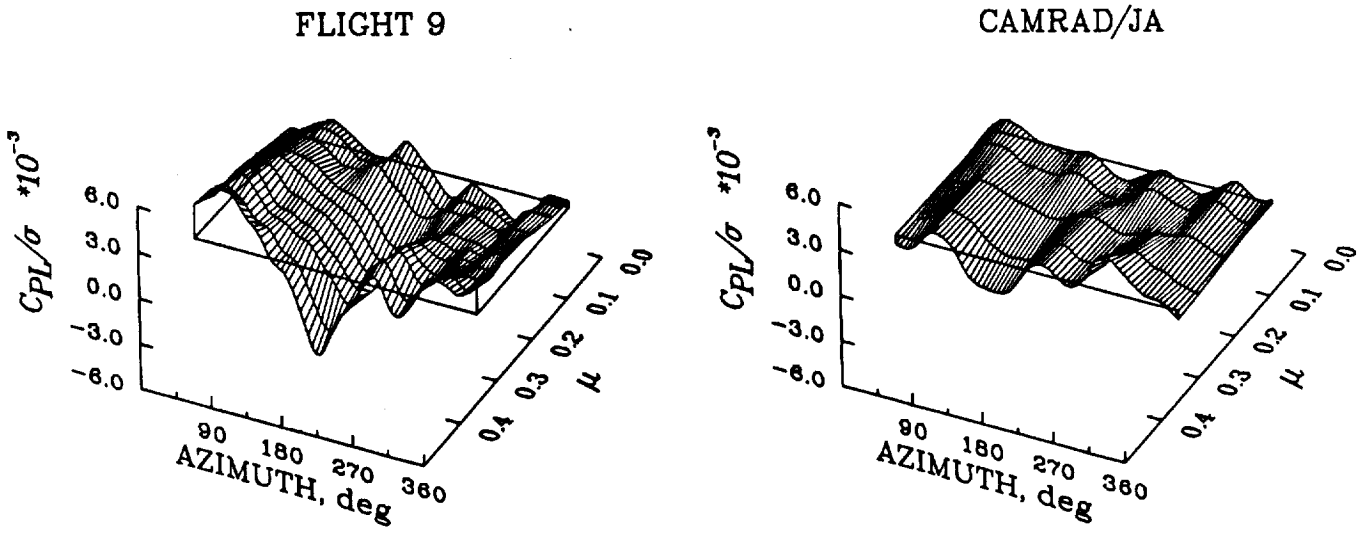

Figure 5. Comparison of oscillatory pitch-link load for the UH-60A as a function of azimuth and advance ratio (Flight 9); 1–12 harmonics.

blade. Pitch-link load measurements were obtained, but no blade torsion measurements were made. No pressure instrumentation was installed for these tests Approximately 5 seconds of data were obtained at each test point and a 20-cycle average has been used for the results shown here. The bandwidth of 128 harmonics is the same as that obtained on the research Puma.

Measurements from the research Puma and UH-60A flight tests illustrate clearly the similarities in torsion loading that were found for five different articulated rotors in reference 1. The first similarity noted is the rapid increase of the pitch-link load with advance ratio. This is seen in figure 2, where the oscillatory (1/2 peak-to-peak) loadings are shown as a function of advance ratio for the swept-tip Puma and UH-60A.

For comparison, the pitch-link load is shown in the nondimensional form

$$\frac{C_{PL}}{\sigma} = \frac{P}{\rho b c \Omega^2 R^3}$$

where P is the pitch-link force, σ the rotor solidity, ρ the density of air, b the number of blades, c the blade chord, Ω the rotor speed, and R the rotor radius. The loading is seen to grow rapidly beyond $\mu = 0.30$.

The azimuthal behavior of the pitch-link load also is quite similar for the two rotors, as is shown in figure 3. This is particularly true on the advancing side of the disk, where each rotor shows a large positive load in the first quadrant that rapidly changes to a negative load in the second quadrant. On the retreating side of the disk, the loading is reduced and differs between rotors.

4 CAMRAD/JA ANALYSIS

The CAMRAD/JA analysis (ref. 4) was used to assess the ability of a current analysis to predict rotor torsional loads. It was further used to identify modeling features within the analysis that are important for the prediction of these loads. CAMRAD/JA was chosen because it is widely used and because it appears to be representative of the better analyses now in use. As an example, the predictions of four analytical methods were compared with flight test data in reference 2 and, although the CAMRAD/JA prediction was not satisfactory for the torsion loading, it was as good or better than any of the other methods examined.

The trim procedure used by CAMRAD/JA for the two aircraft was dictated by the availability of accurate trim measurements. The research Puma was modeled in CAMRAD/JA as a single, isolated rotor. The rotor trim was specified by setting the flight speed, the rotor thrust, the shaft angle, and the first harmonic flapping as measured in flight. In the case of the UH-60A the flapping measurements were not reliable, so it was necessary to model the aircraft with a single main rotor and a single tail rotor for antitorque. Rotor trim was specified by setting the flight speed and requiring that the aircraft forces and moments be balanced for zero sideslip conditions. Both the trim procedure and correlation for the unspecified trim parameters for the two motors are discussed in more detail in reference 5.

5 TORSION LOAD CORRELATION

Baseline Case

Baseline calculations using the CAMRAD/JA model were made over a range of airspeeds for both aircraft. The blade structural deformation in the model is represented by six coupled-flap and lead-lag bending modes, while the torsion deformation is modeled by two torsion modes in the case of the research Puma and by three torsion modes for the UH-60A. The airload computation assumes that the wake is free to distort, which is important at low speed but not at high speed (ref. 5). Two circulation peaks are allowed in the wake model to capture the effects of negative lift at high speed. The blade aerodynamic loading is computed using two-dimensional airfoil tables. A static stall model is used to account for blade stall.

The pitch-link loads calculated by CAMRAD/JA are compared qualitatively with flight test data for the research Puma in figure 4 and for the UH-60A in figure 5. The measured and calculated loads are shown as functions of the blade azimuth and the advance ratio. The experimental measurements are similar for the two rotors and show a buildup in the oscillatory loads as airspeed increases. The calculated pitch-link loads, however, are qualitatively different from measured values for both aircraft.

The pitch-link load correlation at high speed is examined quantitatively in figure 6 for the research Puma and the UH-60A. The azimuthal behavior of the pitch-link loads is poorly predicted for both aircraft. In particular, the positive-negative loading in the first two quadrants of the rotor that is so evident in the flight data is not adequately computed by the analytical model. In addition, the oscillatory pitch-link load amplitude is significantly underpredicted. This underprediction of the oscillatory pitch-link loads occurs at all flight speeds, as shown in figure 7.

Calculation Sensitivity

The CAMRAD/JA calculated pitch-link loads show poor qualitative and quantitative agreement with flight test measurements. This poor agreement suggests that the physics of the torsional loading is not correctly modeled in CAMRAD/JA. It is sometimes possible to gain insight into the physics of rotor loading by looking at which parameters in an analytical model have the greatest influence on the accuracy of the calculation. This approach has been used recently for rotor flap vibratory loads (ref. 5), but in that case the baseline calculations showed reasonably good agreement with flight measurements, which provided confidence in the approach. In the present case, the predicted loads for the baseline case are sufficiently inaccurate that there may be no utility in examining the sensitivity of the calculation to modeling changes. Nonetheless,

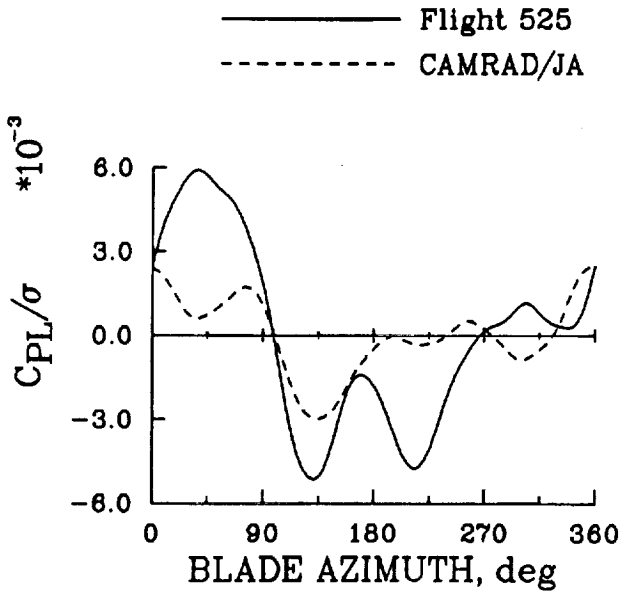

(a) Swept-tip Puma: $\mu = 0.402$ and $C_T/\sigma = 0.070$ (Flight 525)

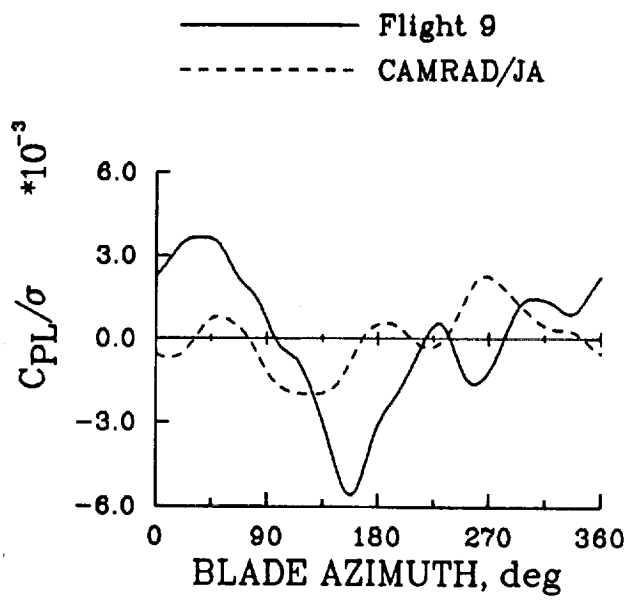

(b) UH-60A: $\mu = 0.355$ and $C_T/\sigma = 0.080$ (Flight 9); 1–12 harmonics.

Figure 6. Comparison of measured and calculated pitch-link load with azimuth.

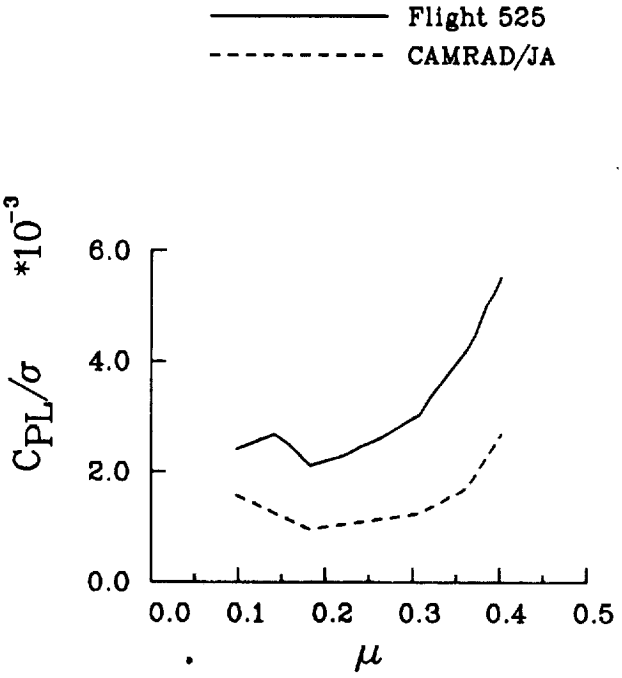

(a) Swept-tip Puma: $C_T/\sigma = 0.070$ (Flight 525)

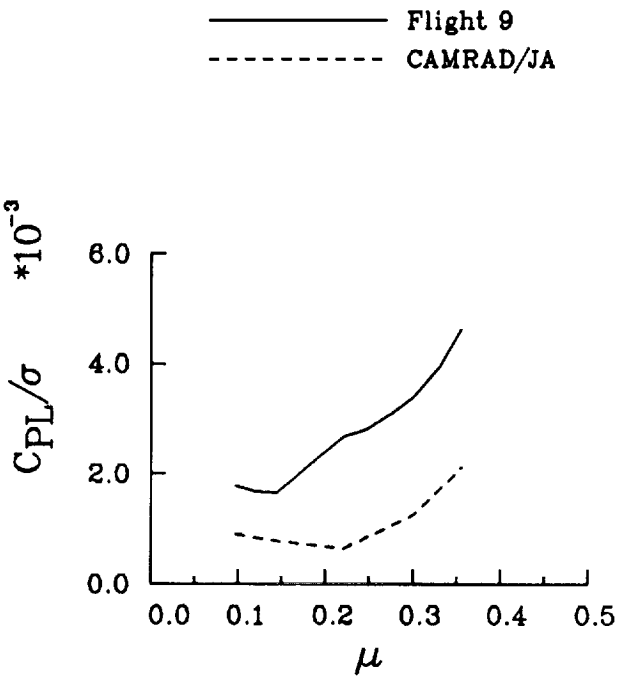

(b) UH-60A: $C_T/\sigma = 0.080$ (Flight 9); 1–12 harmonics.

Figure 7. Comparison of measured and calculated oscillatory pitch-link load with advance ratio;

Table 1. Slope and correlation coefficient values for pitch-link loads and aerodynamic section moments at r/R = 0.95 at high speed; 1–12 harmonics

Puma	Pitch link		Moment	
	m	r	m	r
Free wake	0.29	0.70	0.32	0.59
Prescribed wake	0.29	0.70	0.32	0.59
Straight blade	0.16	0.48	0.29	0.52
No yawed flow	0.25	0.73	0.33	0.63
Boeing dynamic stall	0.30	0.67	0.31	0.56
Johnson dynamic stall	0.30	0.70	0.31	0.59
Single-peak wake model	0.29	0.73	0.32	0.59
Add'l bending/torsion	0.33	0.74	0.31	0.58
No bending modes	0.39	0.84	0.35	0.67
No torsion	–	–	0.37	0.70
No unsteady/ no torsion	–	–	0.03	0.44

the approach of reference 5 will be followed here in the expectation that some insight will be obtained.

Table 2. Slope and correlation coefficient values for UH-60A pitch-link load at high speed; 1–12 harmonics

UH-60A	Pitch link	
	m	r
Free wake	–0.11	–0.24
Prescribed wake	–0.11	–0.24
Straight blade	–0.08	–0.11
No yawed flow	–0.04	–0.10
Boeing dynamic stall	–0.17	–0.36
Johnson dynamic stall	–0.21	–0.42
Single-peak wake model	–0.15	–0.25
Add'l bending/torsion	–0.13	–0.28
No bending modes	–0.30	–0.47

Two measures are used to assess the accuracy of the torsional loading predictions for each of the parametric changes (ref. 5). These measures are obtained by plotting the harmonic cosine and sine coefficients (1–12) of the prediction as a function of the harmonic coefficients of the flight measurement. A least-squares fit is calculated that relates the predicted and measured harmonic coefficients. The first measure of correlation accuracy that is used is the slope of the line, m, which will be unity if the prediction is exact. The second

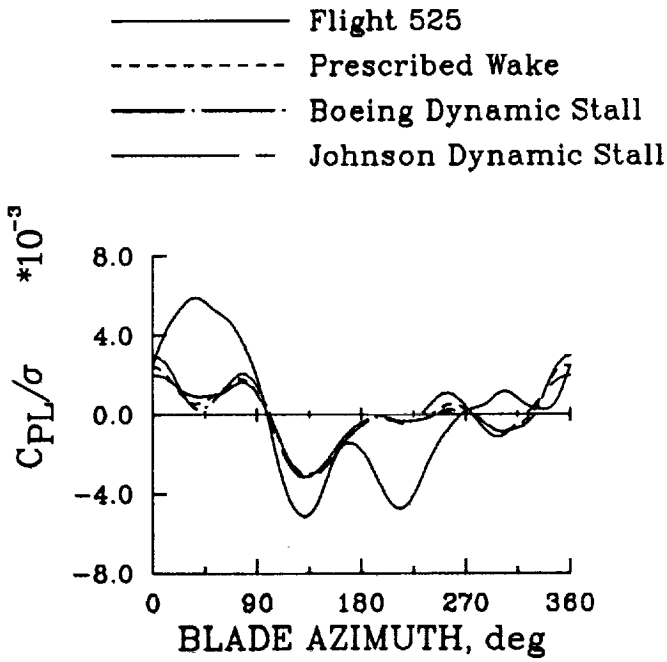

Figure 8. Comparison of predicted and measured pitch-link loads for the Puma; $\mu = 0.402$ and $C_T/\sigma = 0.070$ (Flight 525); 1–12 harmonics.

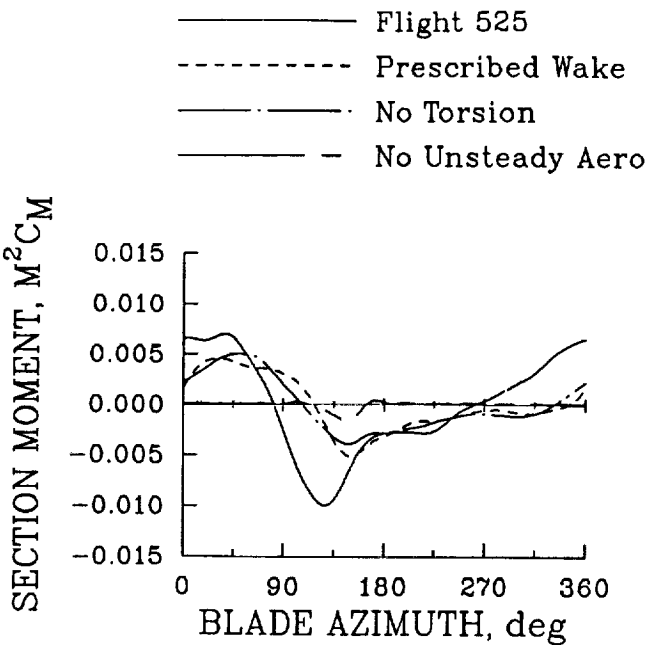

Figure 9. Comparison of predicted and measured aerodynamic section moment for the Puma; $r/R = 0.95$, $\mu = 0.402$, and $C_T/\sigma = 0.070$ (Flight 525); 1–12 harmonics.

measure is the correlation coefficient, r, which is a measure of dispersion. If the prediction matches the measurements exactly, the correlation coefficient also will be one. As an example, the correlation that is shown in figure 6(a) for the research Puma results in a slope of 0.29 and a correlation coefficient of 0.70. The difference in the slope from unity is large, and the correlation coefficient indicates substantial dispersion.

The measures of correlation for the different modeling changes are tabulated in tables 1 and 2 for a high-speed case. Table 1 contains the measures for the Puma pitch-link load and aerodynamic section moment at $0.95R$. Similarly, table 2 contains the measures for the UH-60A pitch-link loads. There are no data available to correlate airload predictions for the UH-60A aircraft. The modeling changes examined in these tables include parameters that affect both the aerodynamic and structural portions of the calculation. A prescribed wake is used rather than the free wake of the baseline model. The "straight blade" case has no aerodynamic or mass offsets from the elastic axis and hence removes the influence of tip sweep. The effects of yawed flow corrections are examined by calculating the airloads under the assumption that the flow is normal to the elastic axis. Two different dynamic stall models are examined. The first, the Boeing dynamic stall model, uses an $\sqrt{\dot{\alpha}}$ stall delay, and the second model, the Johnson model, uses an $\dot{\alpha}$ delay. The single-peak circulation model uses the maximum circulation to calculate the far-wake vortex lattice and tip vortex strengths. The effects of the blade structural modes are examined first by increasing the number of flap and lead-lag bending modes to ten and the number of torsional modes to five; second by removing the flap and lead-lag modes, which results in a rigid, articulated rotor; and third by removing the torsion modes while retaining the flap and lead-lag modes. Finally, the effects of removing unsteady aerodynamics is examined for the case with no torsion modes.

The accuracy measures shown in tables 1 and 2 are, in all cases, poor. In this regard it is difficult to assess the sensitivity of the calculation to modeling changes, as none of these changes shows a clear improvement. However, some insight into the present problem can be gained from these calculations. First, the calculations using the two dynamic stall models have no effect on the accuracy of the calculation, as evidenced by the m and r values in tables 1 and 2. A comparison of the measured and calculated pitch-link loads for the Puma, shown in figure 8, also shows this lack of influence of the dynamic stall model. It is possible that there is no improvement in the predicted torsional loading when including these dynamic stall

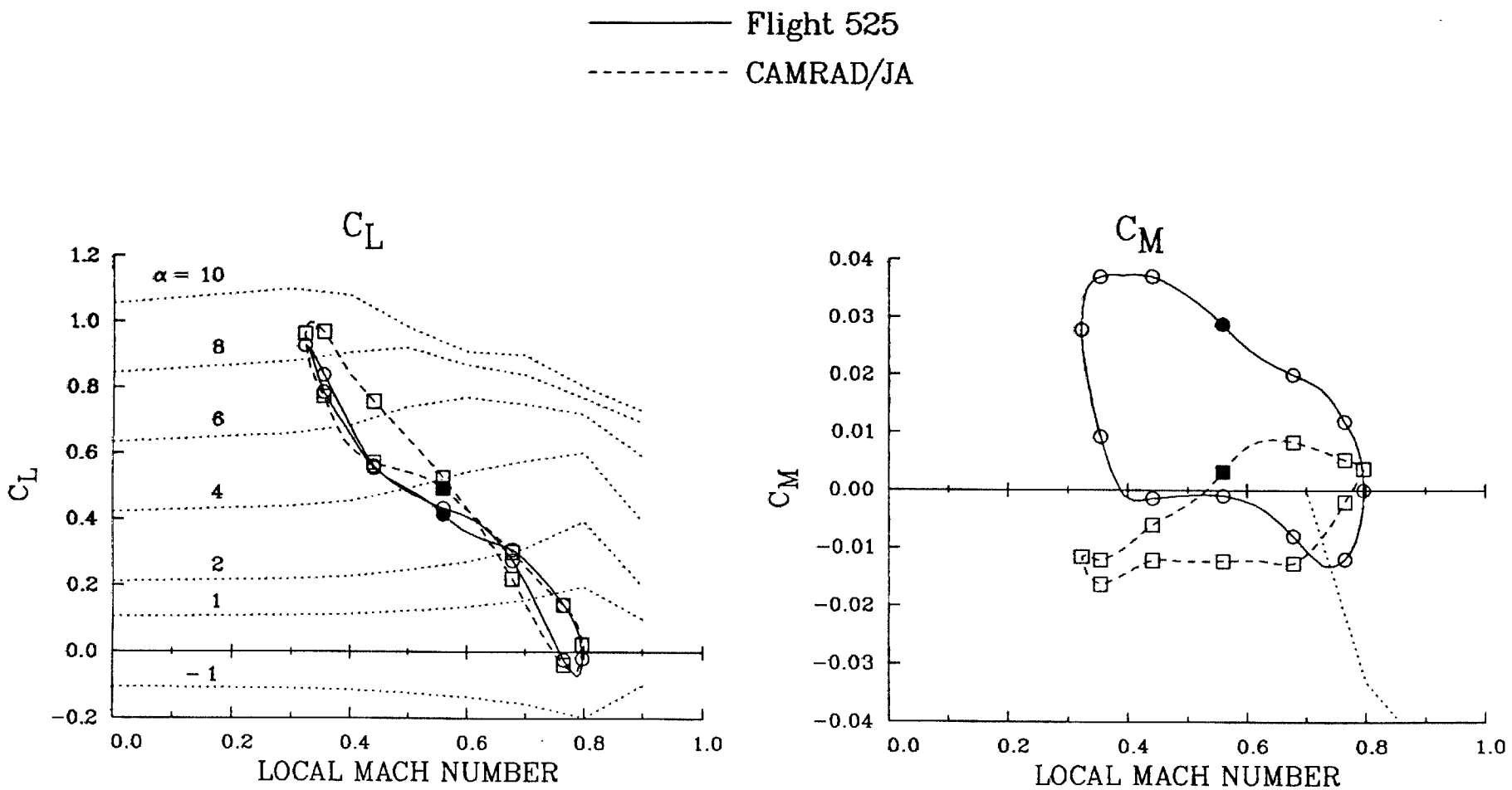

Figure 10. Comparison of predicated and measured aerodynamic section lift and moment as a function of Mach number for the Puma; two-dimensional airfoil data shown as short, dashed line; solid symbols indicate $\phi = 0°$, open symbols every 30°, $r/R = 0.95$, $\mu = 0.402$, and $C_T/\sigma = 0.070$ (Flight 525), 1–12 harmonics. (a) Section lift; (b) section moment.

models because of inadequacies in the models themselves. However, the more likely explanation is that there is very little stall on the rotor disk for these flight conditions; therefore, the dynamic stall model used has no effect.

A second modeling effect that can be seen in table 1 is the effect of removing the unsteady aerodynamic terms. In this case it was necessary to remove the torsion degrees of freedom when the unsteady aerodynamics were removed to obtain a trim solution. Therefore, the "no torsion" case is the appropriate baseline for comparison. Figure 9 demonstrates the influence of unsteady aerodynamics on the section moment at $0.95R$. The case without the blade torsion modes is quite similar to the prescribed-wake case. However, without unsteady aerodynamics, essentially no aerodynamic section moment is predicted to occur. This suggests that improvements in the modeling of unsteady aerodynamic moments may be important in dealing with the present problem. This aspect of the problem was further investigated and is shown in figure 10, where calculated and measured C_L and C_M values are compared for the research Puma at high speed. The steady airfoil characteristics used in the CAMRAD/JA calculation are overplotted in the figure to indicate the operating condition of the airfoil. Over most of the azimuth, the airfoil is below the regime where nonlinear transonic flow becomes important. It is only for a small region on the advancing side of the disk that the steady section moment takes on a nonzero value; over most of the azimuth, the blade is operating at an angle of attack and a Mach number where the steady section moment is zero. From this perspective, nonlinear transonic flows and compressibility effects are unimportant. What does appear to be important is the unsteady loading. The angle of attack varies roughly from $-1°$ to $+9°$, and the CAMRAD/JA lift prediction is quite good. But the section moment is substantially underpredicted and, it seems clear, the effect of unsteady aerodynamics is important.

Hybrid Calculations

It has been shown here that the CAMRAD/JA analysis, a lifting-line-based code, is unable to accurately predict the aerodynamic section moment at the blade tip for the research Puma. It is expected that some improvement should be seen using a CFD-based code that could properly account for the important three-dimensional effects at the tip. Some limited

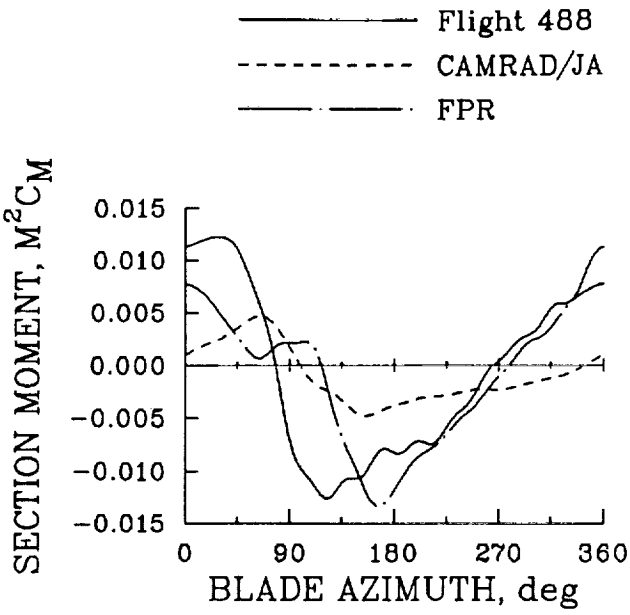

Figure 11. Comparison of CAMRAD/JA and FPR predicted aerodynamic section moment with flight test data for the Puma; $r/R = 0.978$, $\mu = 0.381$, and $C_T/\sigma = 0.070$ (Flight 488); 0–12 harmonics.

calculations have been made in reference 6 that couple the Full-Potential Rotor (FPR) code to CAMRAD/JA; these calculations are compared with the measurements at $0.978R$ shown in figure 11. The hybrid calculations are significantly better than the lifting-line calculations over the retreating side of the disk, but the strong positive-negative loading that is seen in the measurements in the first and second quadrants is not correctly matched. It is important to note, however, that the aerodynamic section moments computed by FPR are not fed back to the CAMRAD/JA analysis through the coupling procedure of reference 6; therefore, the torsional deformations obtained in the CAMRAD/JA solution are based on the CAMRAD/JA section moments. It is possible that a hybrid solution that couples the moment and drag as well as lift would show an improvement in prediction accuracy over the results shown in figure 11.

6 INSIGHT FROM FLIGHT TEST

The CAMRAD/JA analysis is unable to accurately predict the torsion loading that has been measured on the research Puma and UH-60A. The reasons for this are not clear. It is possible to gain some understanding of the parameters that most strongly influence this

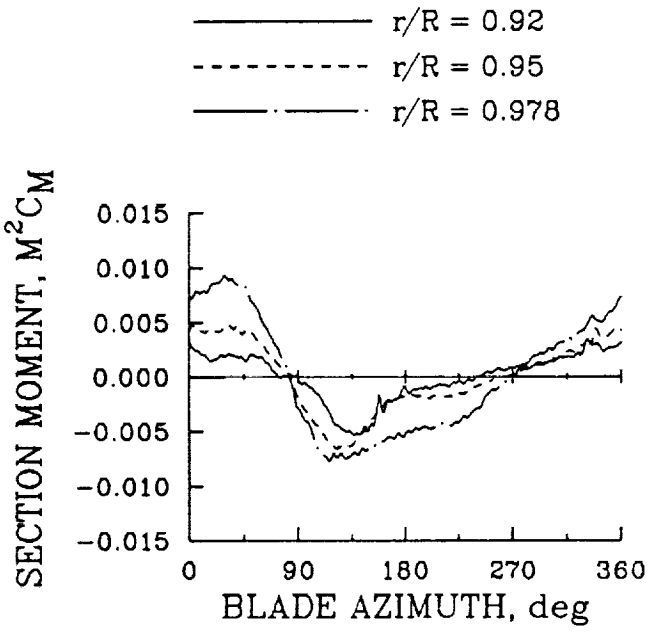

(a) Oscillatory aerodynamic section moment near the blade tip

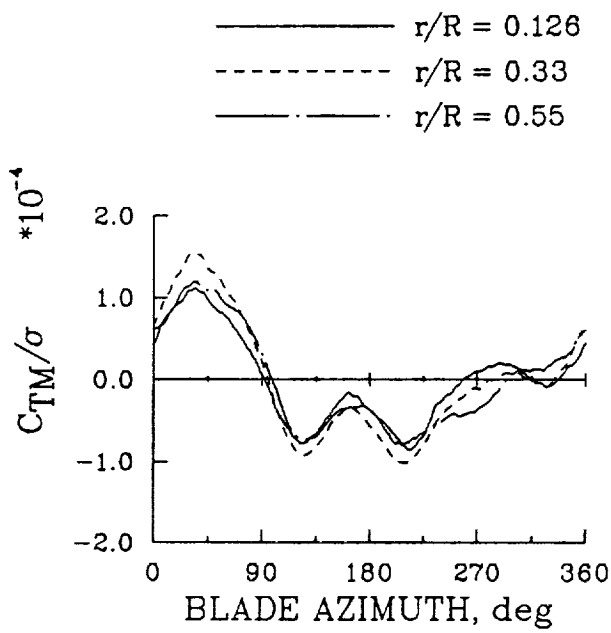

(b) Oscillatory structural torsion moment along the blade span

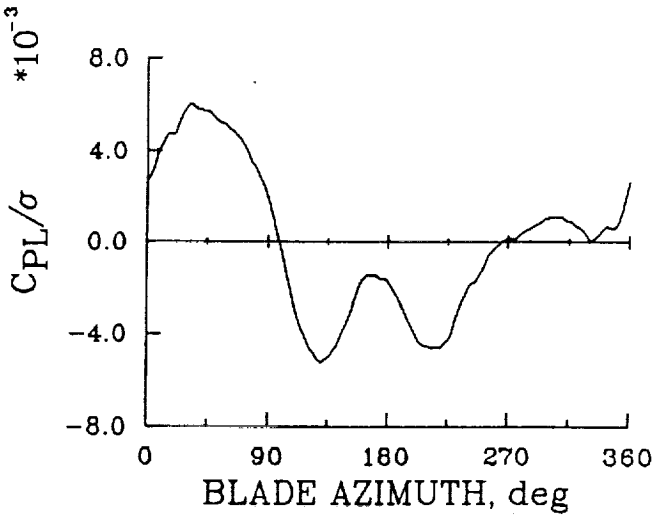

(c) Oscillatory pitch-link load

Figure 12. Flight measurements for the swept-tip Puma; $\mu = 0.402$ and $C_T/\sigma = 0.070$ (Flight 525); 1–64 harmonics.

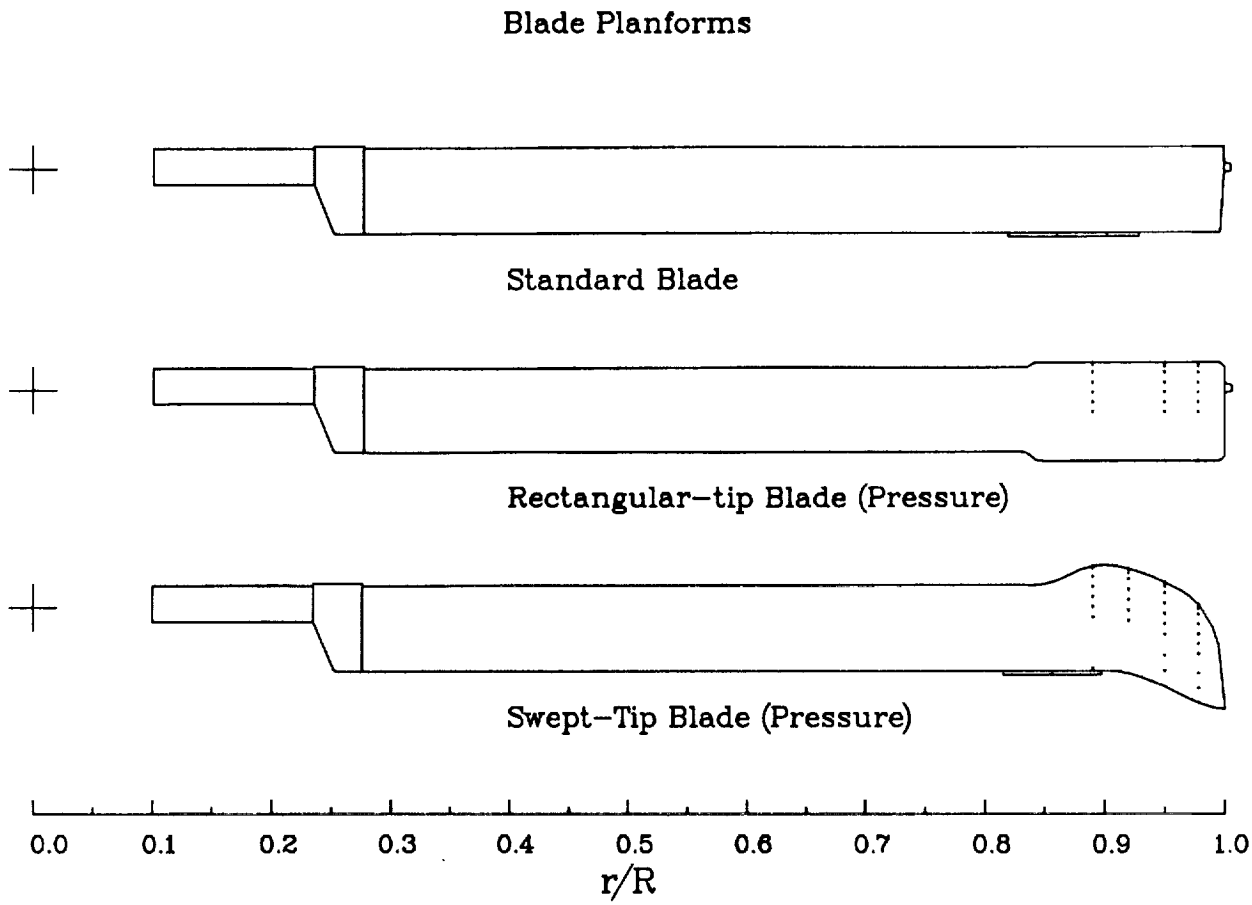

Figure 13. Blade planform for the blades on the mixed-bladed research Puma. Pressure arrays shown by dots.

loading by examining flight test data obtained on the research Puma. This examination process is enhanced, as there are also data available for flights with an unusual mixed-bladed rotor configuration in addition to the testing of the four swept-tip blades that have been used for the correlation.

Swept-Tip Rotor

Data available from the Puma with four swept-tip blades provide strong indications that the pitch-link loads are due mainly to the aerodynamic section moment near the blade tip. Figure 12 shows the aerodynamic section moment near the blade tip, the structural torsion moment inboard on the blade, and the pitch-link load for the swept-tip Puma in high-speed, level flight. Figure 12(a) shows a very rapid growth in aerodynamic section moment near the blade tip. The rate at which the section moments grow with radius indicates that most of the section moment is outboard of $0.90R$. Figure 12(b) shows no significant change in the amplitude or phase of the structural torsion moment with radius. This is especially true over the advancing side of the disk, where the torsion moment is similar in wave form to the aerodynamic section moment. This first-quadrant positive loading, followed by the second-quadrant negative loading, appears to dominate the structural loading. Taken together, these measurements indicate that the aerodynamic section moments on the outer 10% of the blade are the source of the large oscillatory pitch-link load.

Mixed-Bladed Rotor

The mixed-bladed rotor provides a unique set of data from which differences due to planform may be identified. This unusual four-bladed rotor configuration consisted of a swept-tip blade opposed by a gloved, rectangular-tip blade with two standard rectangular blades on either side. The planforms of these blades are illustrated in figure 13. Both the swept-tip blade and

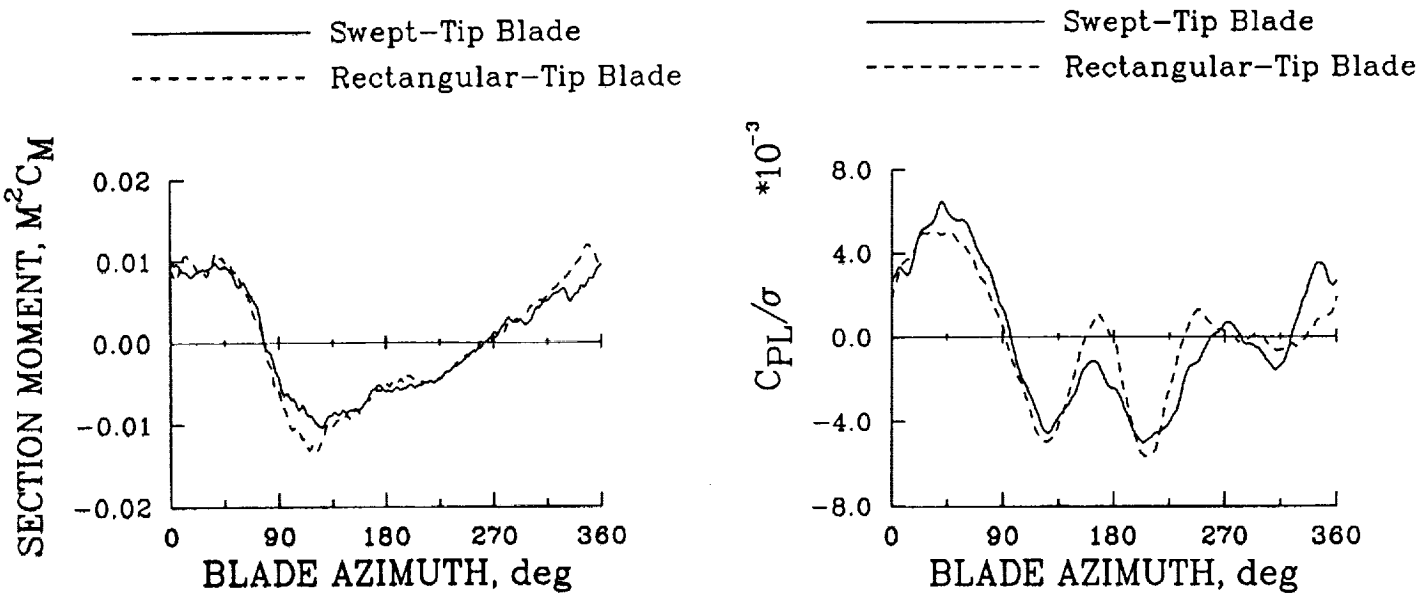

(a) Section moment

(b) Pitch-link load

Figure 14. Comparison of aerodynamic section moment at $0.978R$ and pitch-link load for the swept-tip and rectangular-tip Puma blades; $\mu = 0.376$ and $C_T/\sigma = 0.080$ (Flight 456); 1–64 harmonics.

the gloved, rectangular-tip blade were pressure instrumented. Figure 14 shows the aerodynamic section moment at $0.978R$, and the pitch-link load for the swept-tip and rectangular-tip blades of the mixed-bladed rotor in high-speed flight. The measured section moments for these two blades is very similar. This indicates that the large section moment at the blade tip is not strongly influenced by blade planform. The pitch-link loads for these two blades are also very similar, although the rectangular-tip blade does show slightly greater oscillations on the retreating side.

Lift-Offset Moment

The pitch-link load for the swept-tip blade is affected by the lift-offset moment in addition to the section moment. The lift-offset moment is the section lift times the distance between the feathering axis and the reference location of the section moment. The swept-tip blade has been designed to minimize the integrated effect of this moment by placing the local quarter chord (reference axis) ahead of the feathering axis at the beginning of the swept section. The local quarter chord is then swept aft of the feathering axis outboard of $0.94R$, resulting in spanwise cancellation of the lift-offset moment. Figure 15 shows the CAMRAD/JA prediction of aerodynamic section moment and the lift-offset moment for the swept-tip blade compared to the flight test measurement at zero azimuth. CAMRAD/JA shows good correlation for lift and therefore predicts the lift-offset moment accurately. It is in the prediction of the aerodynamic section moment where CAMRAD/JA falls short. This figure clearly shows how rapidly the measured section moment increases near the blade tip. This rapid increase in section moment is missed completely in the CAMRAD/JA calculation. This sharp gradient with radius near the tip further indicates that an accurate prediction of the loading must incorporate three-dimensional effects.

Measured Chordwise Pressure Distributions

Pressure data available from the mixed-bladed rotor configuration provide additional details of the aerodynamic section moment. Figures 16 and 17 contain the chordwise pressure distribution for the swept-tip and rectangular-tip blades, respectively. The upper surface pressure is shown as a solid line, and the lower surface pressure is shown as a dashed line. The heavy dashed line crossing the ordinates in these figures is the

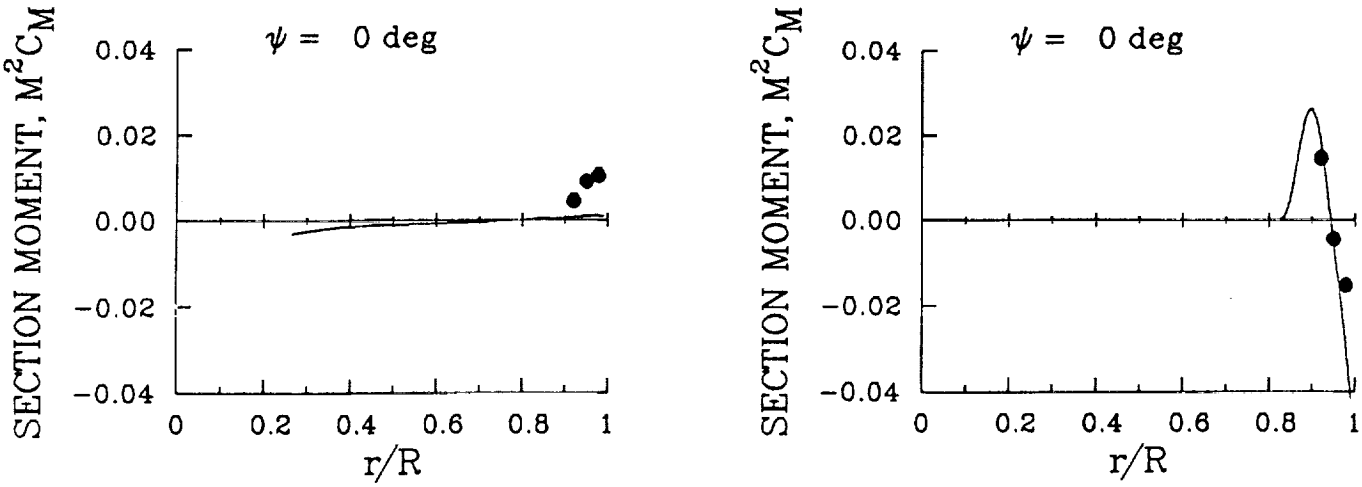

(a) Section moment

(b) Lift-offset moment

Figure 15. Comparison of CAMRAD/JA prediction and flight test data for aerodynamic section moment and lift-offset moment for the Puma at $\psi = 0°$; $\mu = 0.402$ and $C_T/\sigma = 0.070$ (Flight 525); 1–64 harmonics.

critical Mach number line (M = 1), which is the boundary of the supercritical flow regime. Pressure distributions have been selected at the approximate azimuth angles of the maximum nose-up, first zero crossing, the maximum nose-down, and the second zero crossing of the section moment at $0.978R$. On the advancing side of the disk, the rectangular-tip blade shows large areas of supercritical flow and relatively strong shocks as compared to the swept-tip blade, where the compressibility effects are relieved by the sweep. On the retreating side of the disk, where the flow is subsonic, the pressure distributions appear quite similar.

Despite the obvious differences observed between the two blade tips, there are also some similarities; these explain why the integrated section moments of the two tips are so similar. Comparing figures 16(a) and 17(a), the pressure distributions are seen to have high levels of upper surface suction over the airfoil leading edge while the difference in pressure over the aft portion of the airfoil is small. The pressure distribution for the rectangular-tip blade in figure 17(a) shows the leading-edge expansion slightly aft compared to the swept-tip blade, with steep compression typical of transonic flow. Both distributions create a large nose-up section moment. Figure 16(b) shows a pressure distribution typical of two-dimensional non-lifting subcritical flow, and figure 17(b) appears similar, although the rapid compression near the quarter chord indicates the presence of shocks on both the upper and lower surfaces. These distributions result in zero section moment. Figures 16(c) and 17(c) show an increase in lower surface suction over the nose of the airfoil, which results in a nose-down section moment. Figures 16(d) and 17(d) look typical of lifting two-dimensional subcritical flow resulting in zero section moment.

The chordwise pressure distributions during the maximum positive and maximum negative section moments are of particular interest. Figure 18 shows the chordwise pressure distribution at four azimuthal stations over the aft portion of the rotor disk, where the section moment is most positive. From figure 18(a) to 18(b), the section moment is on the rise. The pressure difference along the aft portion of the airfoil is seen to decrease or reverse, causing a nose-up section moment. From figure 18(b) to 18(c), the section moment is fairly constant. From figure 18(c) to 18(d), the section moment has decreased. The leading-edge suction has decreased, and the lower surface pressure is approaching the upper surface pressure. Both section lift and section moment are rapidly approaching zero. Figure 19 shows the chordwise pressure distribution at four azimuthal stations over the advancing side of the rotor disk, where the section moment is most negative. In figure 19(a) the lift is slightly negative; the lower surface leading-edge suction over the front of the airfoil exceeds the upper surface suction, causing a negative section moment. From figure 19(a) to 19(b), the pressure difference over the aft portion of

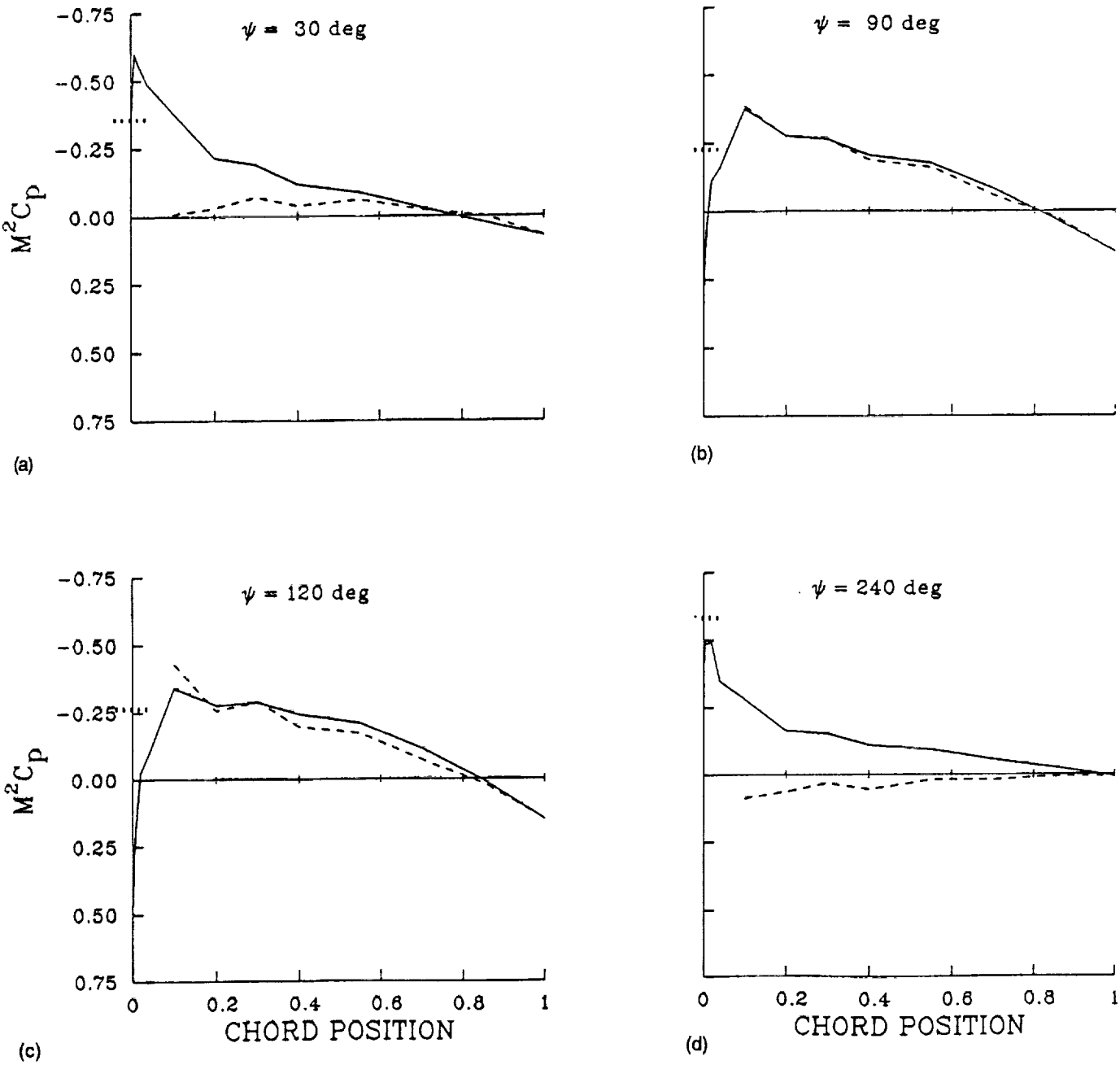

Figure 16. Chordwise pressure distribution for the swept-tip Puma blade; $r/R = 0.978$, $\mu = 0.376$ and $C_T/\sigma = 0.080$ (Flight 456); 1–64 harmonics. (a) Maximum nose up, (b) first zero crossing, (c) Maximum nose down, (d) second zero crossing.

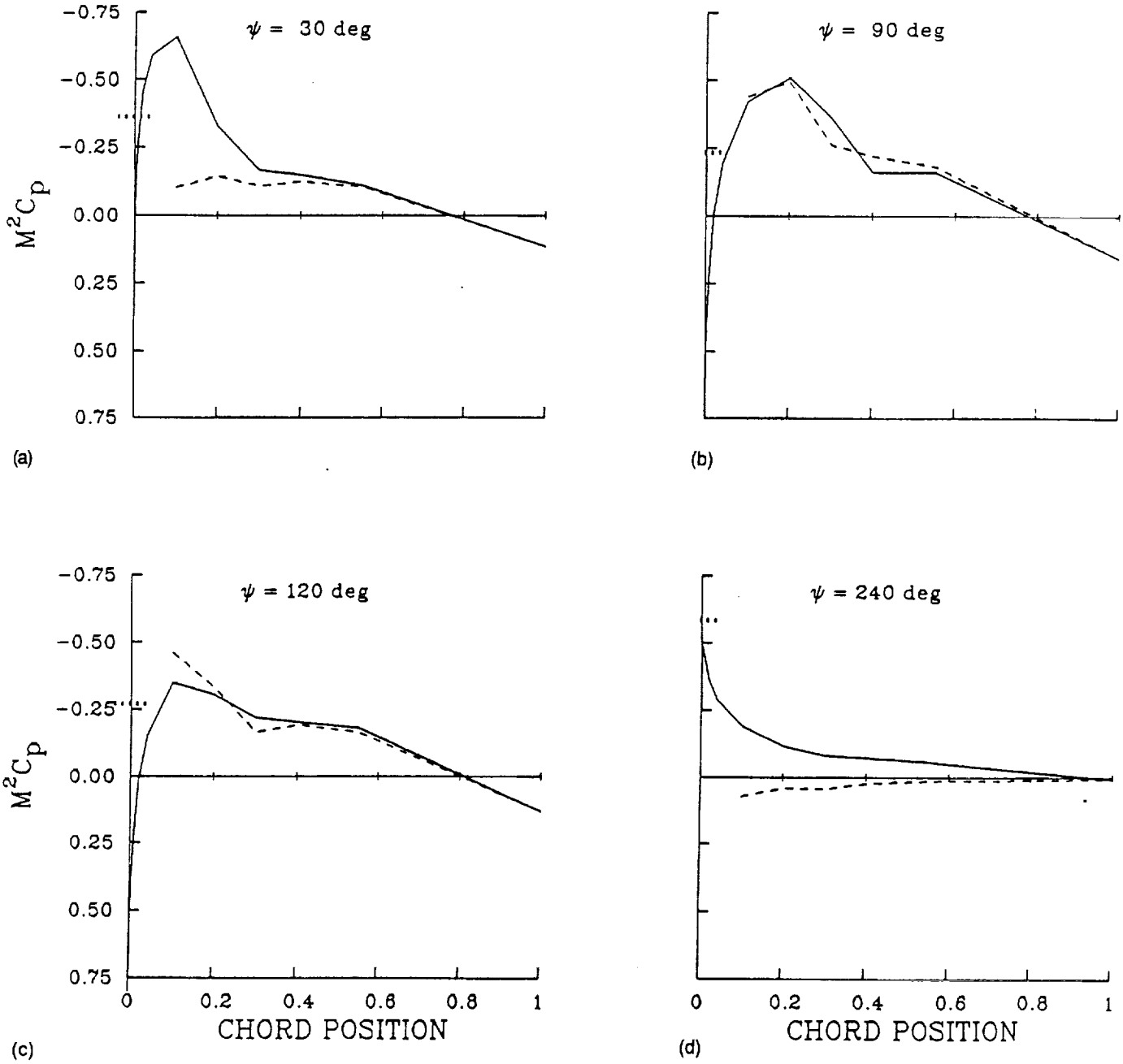

Figure 17. Chordwise pressure distribution for the rectangular-tip Puma blade; $r/R = 0.978$, $\mu = 0.376$ and $C_T/\sigma = 0.080$ (Flight 456); 1–64 harmonics. (a) Maximum nose up, (b) first zero crossing, (c) Maximum nose down, (d) second zero crossing.

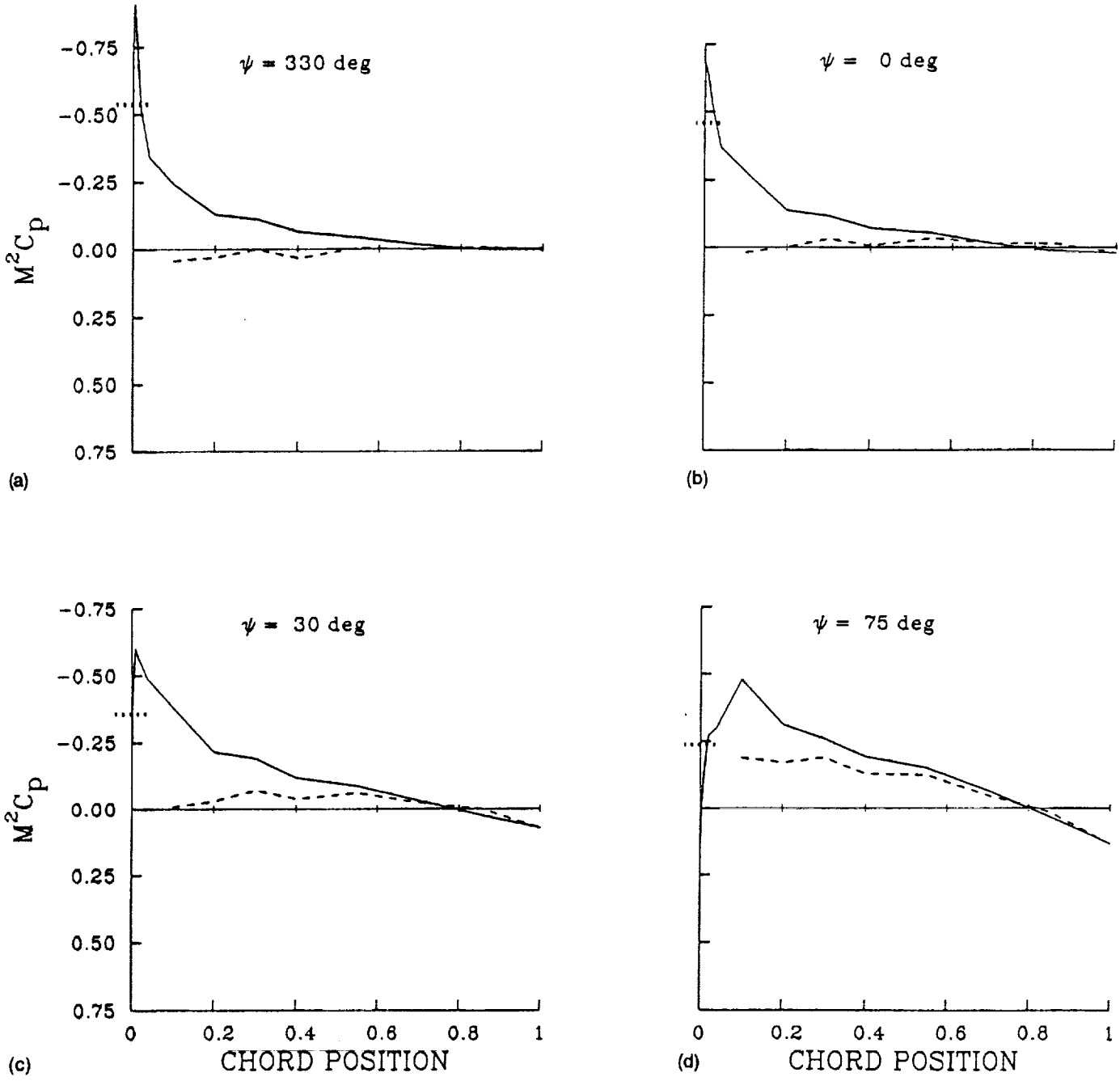

Figure 18. Chordwise pressure distribution for the swept-tip Puma blade through the positive section moment peak; $r/R = 0.978$, $\mu = 0.376$ and $C_T/\sigma = 0.080$ (Flight 456); 1–64 harmonics.

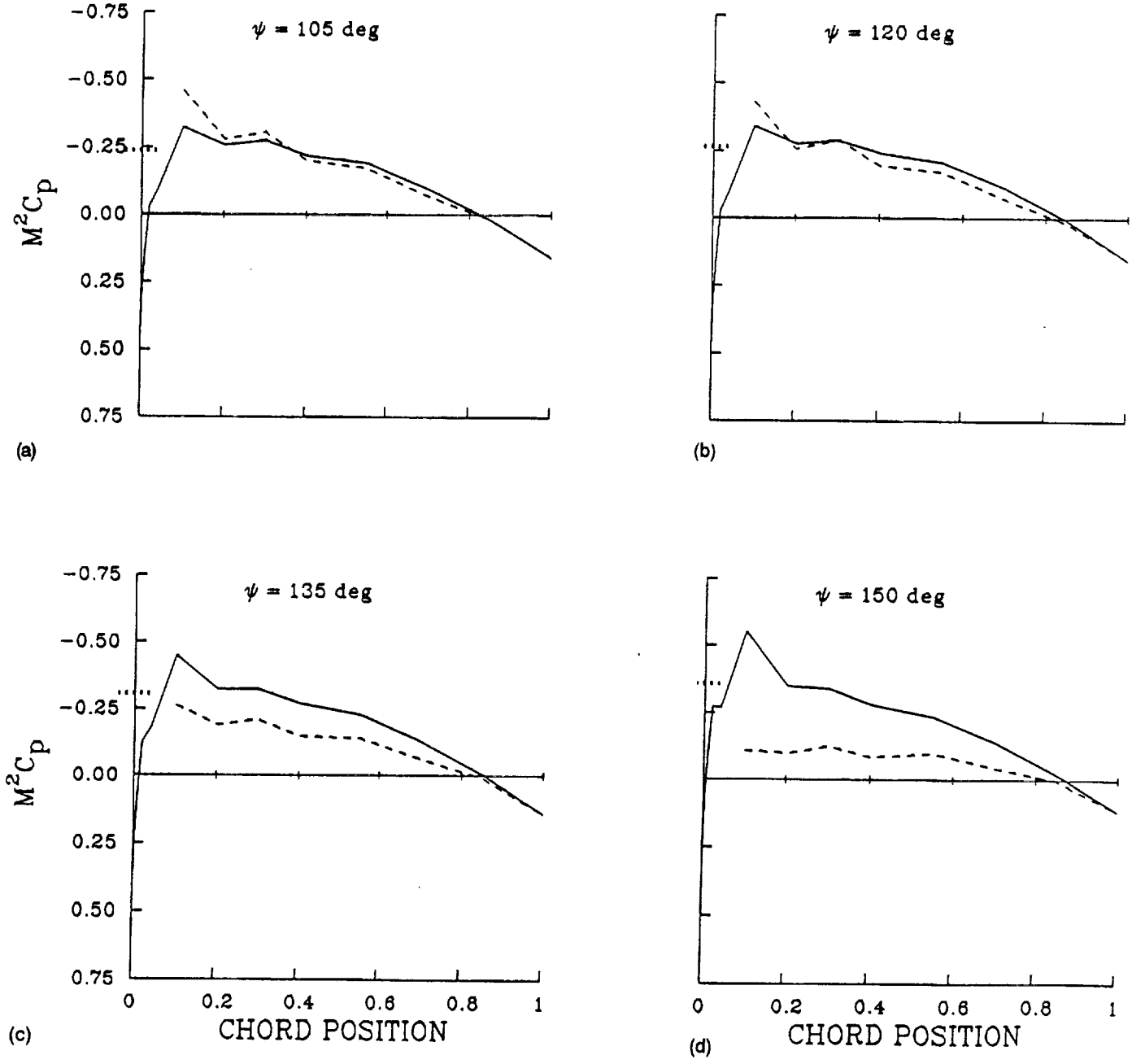

Figure 19. Chordwise pressure distribution for the swept-tip Puma blade through the negative section moment peak; $r/R = 0.978$, $\mu = 0.376$ and $C_T/\sigma = 0.080$ (Flight 456); 1–64 harmonics.

the airfoil has grown, causing an increase in the nose-down section moment. From figure 19(b) to 19(c), the upper surface suction over the nose of the airfoil has grown and the difference in pressure over the aft portion has grown. These effects cause opposite section moments; the net result is little change in the section moment. From figure 19(c) to 19(d), the increase in the pressure difference over the aft portion of the airfoil has increased faster than the increase in upper surface suction over the nose, resulting in a decrease in the nose-down section moment. The aerodynamic loading shown in these figures is not completely understood. It does seem clear, however, that the correct calculation of these section moments will require an accurate accounting of both three-dimensional and unsteady effects. This remains a challenge in the development of comprehensive methods for rotor loads.

7 CONCLUDING REMARKS

Flight test data and the CAMRAD/JA analysis have been used in this paper to examine the buildup of the blade torsional loads and the control system loads that are observed at high speed for a number of articulated rotors. It is shown here that it is not possible to accurately predict these high-speed loads; this is clearly a deficiency of present analytical methods. It is possible, however, to obtain substantial insight into the high-speed loading problem using both measurements and analysis.

The detailed aerodynamic measurements made on the research Puma show that the torsional loading is characterized by large positive section moments in the first quadrant, with a rapid reversal of load so that the section moment is negative in the second quadrant. The section moment then returns to its large positive value in a gradual manner around the retreating side of the disk. It is believed that this loading is directly related to:

1. The three-dimensional character of the flow over the rotor blade tip.

2. Unsteadiness in the aerodynamic loading induced by the large cyclic pitch motion and elastic torsion.

From the present examination it is also possible to suggest features of the rotor loading that are not important for the prediction of these high torsional loads:

1. The specific geometry of the blade tip has only a minor effect on this loading.

2. Compressibility is not important in modeling of the rotor unsteady airloads for this torsional loading problem.

3. The angles of attack of the blade tip are not large for the lift levels examined, and dynamic stall does not play a part in this loading.

4. The effects of yawed flow at the blade tip do not play a significant role in this loading.

5. The structure of the rotor wake has only a minor effect on this aspect of the rotor loading.

8 REFERENCES

1. Bousman, William G.: The Response of Helicopter Rotors to Vibratory Airloads. J. American Helicopter Society, vol. 34, no. 4, Oct. 1990, pp. 53–62.
2. Young, Colin; Bousman, William G.; Maier, Thomas H.; Toulmay, François; and Gilbert, Neil: Lifting Line Predictions for a Swept Tip Rotor Blade. American Helicopter Society 47th Annual Forum Proceedings, May 1991, pp. 1345–1370.
3. Buckanin, Robert M.; Gould, Warren; Losier, Paul W.; Downey, David A.; Lockwood, Roy; Webre, James L.; Hagen, John F.; Cason, Randall W.; and Young, Christopher J.: Rotor System Evaluation, Phase 1. AEFA Project No. 85–15, March 1988.
4. Johnson, Wayne: CAMRAD/JA: A Comprehensive Analytical Model of Rotorcraft Aerodynamics and Dynamics; Johnson Aeronautics Version; Volume I, Theory Manual. Johnson Aeronautics, Palo Alto, California, 1988.
5. Bousman, William G.; and Maier, Thomas H.: An Investigation of Helicopter Rotor Blade Flap Vibratory Loads. American Helicopter Society 48th Annual Forum Proceedings, June 1992, pp. 977–999.
6. Strawn, Roger C.; and Bridgeman, John O.: An Improved Three-Dimensional Aerodynamics Model for Helicopter Airloads Prediction. AIAA 29th Aerospace Science Meeting, Jan. 1991.

REPORT DOCUMENTATION PAGE

Form Approved
OMB No. 0704-0188

1. AGENCY USE ONLY *(Leave blank)*	2. REPORT DATE	3. REPORT TYPE AND DATES COVERED
	October 1993	Technical Memorandum

4. TITLE AND SUBTITLE

An Examination of the Aerodynamic Moment on Rotor Blade Tips Using Flight Test Data and Analysis

5. FUNDING NUMBERS

505-59-52

6. AUTHOR(S)

Thomas H. Maier and William G. Bousman

7. PERFORMING ORGANIZATION NAME(S) AND ADDRESS(ES)

Aeroflightdynamics Directorate, U.S. Army Aviation and Troop Command, Ames Research Center, Moffett Field, CA 94035-1000

8. PERFORMING ORGANIZATION REPORT NUMBER

A-93047

9. SPONSORING/MONITORING AGENCY NAME(S) AND ADDRESS(ES)

National Aeronautics and Space Administration
Washington, DC 20546-0001 and U.S. Army Aviation and Troop Command, St. Louis, MO 63120-1798

10. SPONSORING/MONITORING AGENCY REPORT NUMBER

NASA TM-104006
USAATCOM TR-92-A-014

11. SUPPLEMENTARY NOTES

Point of Contact: Thomas H. Maier, Ames Research Center, MS 215-1, Moffett Field, CA 94035-1000 (415) 604-3643

12a. DISTRIBUTION/AVAILABILITY STATEMENT

Unclassified – Unlimited
Subject Category – 02

12b. DISTRIBUTION CODE

13. ABSTRACT ***(Maximum 200 words)***

The analysis CAMRAD/JA is used to model two aircraft, a Puma with a swept-tip blade and a UH-60A Black Hawk. The accuracy of the analysis in predicting the torsion loads is assessed by comparing the predicted loads with measurements from flight tests. The influence of assumptions in the analytical model is examined by varying model parameters and comparing the predicted results to baseline values for the torsion loads. Flight test data from a research Puma are used to identify the source of torsion loads. These data indicate that the aerodynamic section moment in the region of the blade tip dominates torsion loading in high-speed flight. Both the aerodynamic section moment at the blade tip and the pitch-link loads are characterized by large positive (nose-up) moments in the first quadrant with rapid reversal of load so that the moment is negative in the second quadrant. Both the character and magnitude of this loading are missed by the CAMRAD/JA analysis.

14. SUBJECT TERMS

Pitch-link loads, Aerodynamic moment pitching, Helicopter aerodynamics

15. NUMBER OF PAGES

22

16. PRICE CODE

A03

17. SECURITY CLASSIFICATION OF REPORT	18. SECURITY CLASSIFICATION OF THIS PAGE	19. SECURITY CLASSIFICATION OF ABSTRACT	20. LIMITATION OF ABSTRACT
Unclassified	Unclassified		